Characteristics of polysilicon resonant microbeams*

J D Zook and D W Burns
Honeywell Sensor and System Development Center, Bloomington, MN 55420 (USA)

H Guckel, J J Sniegowski**, R L Engelstad and Z Feng
Wisconsin Center for Applied Microelectronics, University of Wisconsin, Madison WI 53706 (USA)

(Received January 21 1992, accepted April 2, 1992)

Abstract

Polysilicon resonant microbeams can be used as strain-sensitive elements to replace conventional silicon piezoresistors in precision sensor applications, such as pressure sensors and accelerometers These elements are combined with conventional silicon diaphragms or flexures with a proof mass to convert pressure or acceleration directly into a frequency output Vacuum-enclosed resonant microbeam elements 200 or 400 μm long, 45 μm wide and 1 8 μm thick have been fabricated using LPCVD mechanical-grade polysilicon at the University of Wisconsin Q-values determined using gain/phase analysis are typically over 25 000 Lower Q-values are primarily the result of residual gas in the cavity Closed-loop operation from −60 to 180 °C using piezoresistive sensor and electrostatic drive has been achieved with automatic gain control (AGC) to prevent overdrive The characteristic resonance frequencies of the beams have been measured, with 550 kHz, 1 2, 2 2 and 5 2 MHz being typical of the frequencies of the one-dimensional bending modes for the 200 μm length These measurements of the multiple resonance frequencies of a single beam provide a means of testing mathematical models of the dynamic behavior as well as determining the residual beam stress The one-dimensional (1D) differential equation of motion of a doubly clamped single-span beam with an axial load can be solved analytically for lateral natural frequencies and mode shapes These 1D solutions have been verified by 3D finite-element methods In addition, the finite-element models are used to identify both lateral and torsional modes The closed-form solutions agree closely with the numerical results and the experimental data

Introduction

Requirements for sensors and transducers are increasingly demanding in industrial, commercial and residential control applications, as well as in commercial and military aviation systems There is an increasing trend toward more autonomy and higher functionality and at the same time sensors must be increasingly cost effective and reliable To meet these requirements, it is important that a sensor provide digital output for direct interfacing to digital control systems and data highways It is now well accepted that resonant sensors offer significant advantages for integrating the sensing and digitization functions in the same monolithic structure by providing a frequency output that is readily converted to a digital sensor output

Resonant elements, such as vibrating wires, diaphragms and cylinders, have been used in sensor applications for the past three decades In 1970, Sperry (now Honeywell) combined a resonant Cu–Be diaphragm with digital electronics to produce the first digital pressure sensor [1] Resonant sensors still offer the highest resolution, performance, long-term stability and reliability available today The stability is determined only by the mechanical properties of the resonator material, not by the stability of the electronic circuits The frequency output provides high-level signals and is less sensitive to spurious or parasitic influences than capacitive or piezoresistive devices The ubiquitousness of quartz wristwatches shows that batch-fabricated resonant structures, together with their associated oscillator and digital electronic circuits, can be very low in cost and high in performance Recent advances in silicon micromachining technology

*Based on a paper presented at the 6th International Conference on Solid-State Sensors and Actuators (Transducers '91), San Francisco, CA, USA, June 24–28, 1991

**Present address Sandia National Laboratories, Albuquerque, NM 87185 USA

0924-4247/92/$5 00

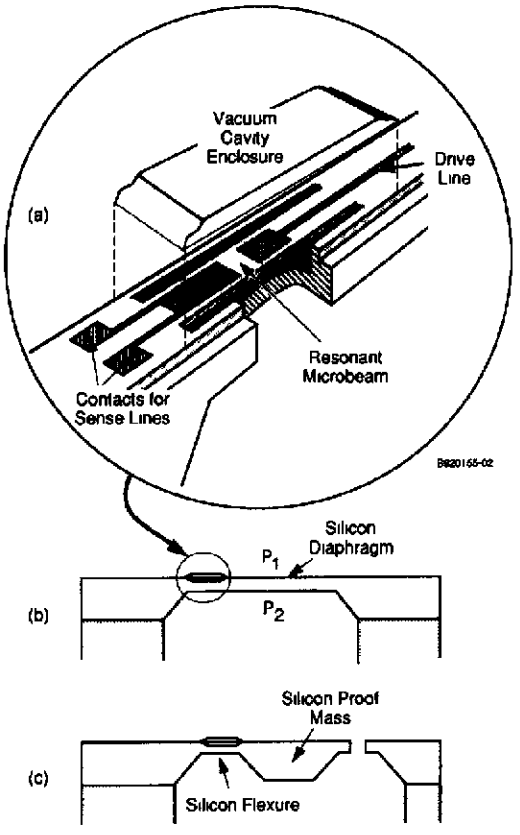

Fig 1 Resonant microbeams (a) Cross-sectional view of polysilicon beam attached to silicon diaphragms (b) or flexures (c) In (b), when the pressure P_1 exceeds P_2 the diaphragm bends downward, increasing the resonance frequency of the microbeam, represented by the line in the middle of the symbol In (c), an upward acceleration deflects the proof mass downward, causing a frequency increase The microbeam is sealed in an integral vacuum enclosure to prevent gas damping

have led to silicon resonant structures [2–12] that have been proposed for a variety of transducer applications

The resonant microsensors demonstrated at the University of Wisconsin [7–11] are fabricated by depositing and patterning fine-grain low-tensile-strain polysilicon thin films and sacrificial layers, resulting in a free-standing silicon beam sealed inside a polysilicon shell (Fig 1) The polysilicon process was originally developed for nonresonant pressure sensors and appears to have the high stability, controllability and repeatability required for high-performance digital transducers The vacuum within the polysilicon shell is achieved by reactive sealing [7–11, 20]

The electrode arrangement is shown schematically in Fig 2 The beam is driven at resonance by a sinusoidal voltage which causes it to be alternately attracted to the top electrode on the shell or the bottom electrode (the substrate), which are biased oppositely with respect to the beam electrode Alternate bias and drive schemes have been described in ref 10 The drive electrode, sense resistor and top electrode are fabricated by ion implantation into the polysilicon, which is a semi-insulator The implanted resistor values are not critical, since the sensor output is at the mechanical resonance as long as the oscillation is maintained The piezoresistive sense resistor, implanted on the upper surface near one end of the beam, changes its resistance when the beam deflects In principle, the stability of the sensor output depends only on the mechanical properties of the

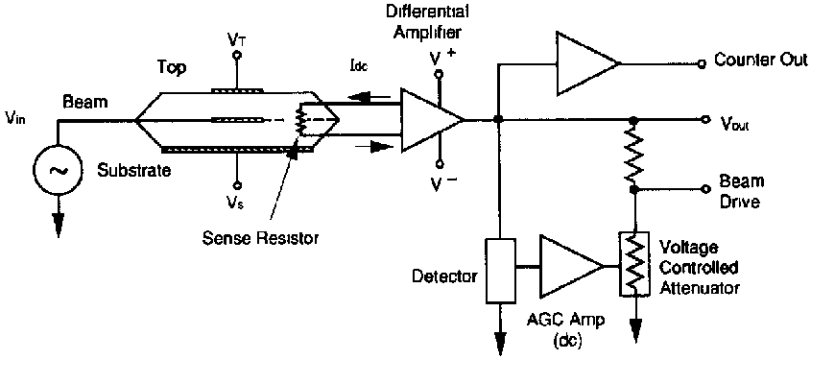

Fig 2 Microbeam test circuit For open-loop tests, the beam electrode (see Fig 1(a)) is driven by an external oscillator at the test frequency The differential amplifier amplifies the a c signal from the piezoresistive sense resistor For closed-loop operation, an automatic gain control (AGC) circuit is used to maintain constant amplitude and prevent overdriving the beam Open-loop tests (1) disable AGC, (2) measure gain = V_{out}/V_{in} vs frequency, drive amplitude Closed-loop tests (1) enable AGC, (2) connect beam drive, (3) measure frequency vs strain, temperature

structure, and does not depend on the stability of the piezoresistor

Figure 2 also schematically illustrates the circuit used for both open-loop measurements of gain and Q and closed-loop measurements of gage factor, temperature sensitivity and frequency stability The amplifier amplifies the piezoresistive signal resulting from the beam vibration and must have sufficient gain so that, at resonance, the overall open-loop gain generously exceeds unity to insure that the circuit will oscillate in closed-loop operation As discussed below, only a small voltage is needed to drive the beam (a few millivolts) For closed-loop tests, an automatic gain control (AGC) circuit is used to maintain a constant-amplitude variable-frequency output (V_{out}) This sinusoidal output is conditioned to provide output to a frequency meter

Resonator characteristics

The resonant response of the microbeam was characterized using a gain–phase analyzer (Hewlett Packard 4194A) with capabilities from 10 Hz to 100 MHz A typical example of the analyzer output is shown by the dashed lines in Fig 3 The gain amplitude shows a sharp resonance and the phase has a rapid decrease in the vicinity of the resonance Either of the curves can be used to determine Q The solid lines show the same device, under the same drive conditions (3 mV rms), but with the gain–phase analyzer directly probing one side of the piezoresistor The devices, though very stable, are extremely strain-sensitive (as intended)

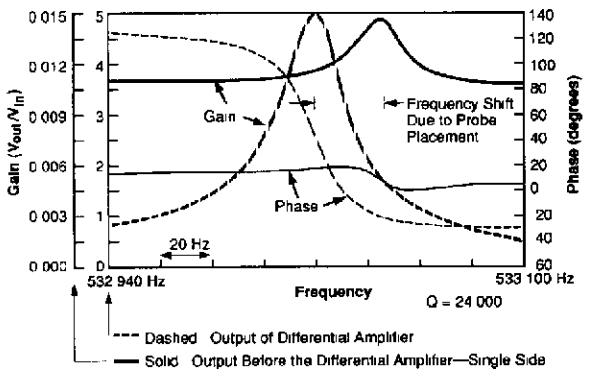

Fig 3 Typical resonant response The dashed lines show the output after the differential amplifier The solid lines show the gain measured before amplification

and it was verified that the frequency shift between the dashed set of curves and the solid curves was due to the pressure applied by the probe tip to the chip, which was rigidly bonded on a ceramic package Packaging-induced temperature coefficients and hysteresis are to be expected for this sensor, as for any pressure sensor where ppm accuracies are important

The microbeam resonators are also sensitive to drive conditions as illustrated in Fig 4 for a lower-Q device As the drive voltage is increased, the resonance frequency shifts to a higher value, leading to hysteresis depending on the direction of the frequency scan This behavior is typical of a 'hard' resonator in which stiffness increases with amplitude [21] In spite of the low voltages required for linear operation, it has been found that the devices are very rugged and are not damaged by large voltages (10 20 V) applied to the drive electrodes

An important issue regarding the use of polysilicon as a resonant element concerns the quality factor, Q, for mechanical resonance Since polysilicon consists of large numbers of grain boundaries, there is a concern [13] that dissipative mechanisms introduced by the grain boundaries would render the polysilicon unusable However, work at the University of Wisconsin [14, 6–10], as well as the present work, demonstrates that polysilicon can have surprisingly high Q values, typically $Q \sim 25\,000$

If the vacuum in the shell were perfect, Q would be determined only by the resonator material and method of fabrication The intrinsic material loss mechanism for beam resonators involves the thermoelastic effect first observed by Zener (see ref 15) Because of the operational frequencies and dimensions of micromechanical flexural resonators, the thermoelastic effect can be a significant dissipation mechanism [15, 16] The thermoelastic effect has its origin in thermal energy flow from compressed regions to rarefaction regions (i e , corresponding to the bottom half and the top half of the beam center for a beam deflected upwards) The significance of the mechanism can be determined by calculation of the characteristic damping frequency of the resonance beam [15] For the present devices the operational frequency is well below this limit, and it is clear that this damping mechanism is not a factor Further discussion of intrinsic loss mechanisms in

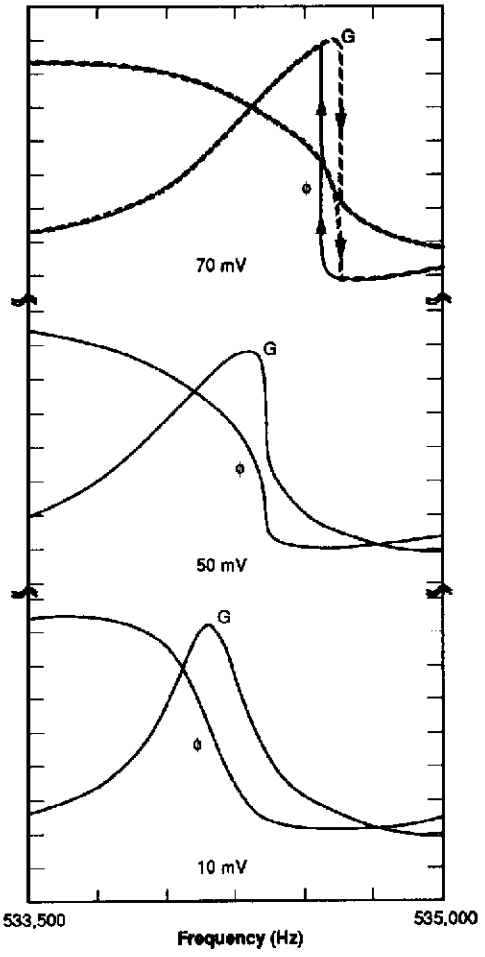

Fig 4 Nonlinear behavior of microbeam resonators As the drive amplitude is increased, the resonance shifts to higher frequencies, and the frequency response becomes asymmetric, eventually showing amplitude discontinuities and hysteresis as the frequency is swept ----, Increasing frequency, ——, decreasing frequency Drive voltage = 10, 50, 70 mV rms, G = gain (0 5/div), ϕ = phase (20°/div)

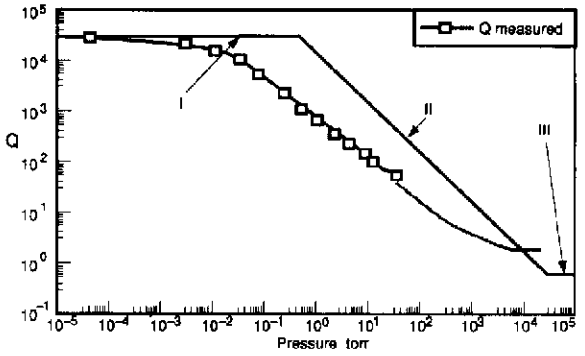

Fig 5 Quality factor vs external pressure for a 200 μm long, 40 μm wide microbeam The theoretical predictions of Q are designated by the solid lines in the three regions Region I corresponds to the observed limit Q of the resonator, II is the region of momentum damping by collisions with individual gas molecules while III is the region of viscous damping

construction materials is given by Hok and Gustafsson [13] We assume that the basic loss mechanism in our devices is due to end losses arising from uncancelled shear forces and moments at the end supports, which transfer energy from the beam to the substrate It is well known that this loss can be minimized by the use of a dual-beam tuning-fork configuration, or a sophisticated isolator structure before the beam mount [17–19, 22] Such structures would complicate fabrication and introduce complicated modes into the frequency mode spectrum [23] Instead, the resonance frequency of the microbeam was designed to be much greater than the vibrational modes in the supporting structure This reduces effective coupling losses to the substrate and allows the high Q-values to be obtained

Residual pressure in the microbeam enclosure can have a strong detrimental effect on Q, as illustrated in Fig 5 The measured data were obtained by carefully fracturing the cover of a device using a sharp probe tip without damaging the resonant beam The device was then monitored *in situ* in a vacuum chamber while the pressure was decreased by pumping The measurement of Q was done by applying a voltage pulse, and observing the ring-down [10] Above 100 mTorr, no ringing was observed As the pressure decreased, Q increased until the limiting value was reached Testing devices with low Q in this way produced essentially identical results [10] The results imply that the root cause of Q variations was a variable cavity vacuum resulting from the LPCVD silicon-nitride sealing process The sealing process has since been modified slightly and seals with high vacuum can be obtained consistently The variation of Q with pressure for resonant beams, diaphragms and tuning forks is well known [3, 4, 16, 18] In the low-pressure region (region II of Fig 5) the gas is still rarefied to the point that the gas molecules are not interacting with each other Damping occurs by momentum transfer during collisions between individual gas molecules and the beam Newell [24] applied the model of Christian [25] to miniaturized cantilevers In this model the rate of momentum transfer is proportional to the difference in velocity between the gas molecules and the resonator The

damping is proportional to the gas pressure, P, and yields a Q given by

$$Q = \left(\frac{\pi}{2}\right)^{3/2} \rho b f_r \left[\frac{RT}{M_0}\right]^{1/2} \left(\frac{1}{P}\right) \quad (1)$$

where R is the universal gas constant, T is absolute temperature, M is the molecular mass of the gas, ρ is the density of the beam material, h is the beam thickness and f_r is the resonance frequency

There is rough agreement between eqn (1) and experiment, as shown in Fig 5 The most probable failure of the theory is the assumption of free space surrounding the resonating structure The close proximity of the beam to the shell means that the gap is much less than the mean free path length of the gas molecules, causing rapid reflection of the gas molecules and thereby increasing the damping rate In addition, the equation is based upon classical gas equations The validity of that assumption as applied to these structures has not been established This equation has been criticized as inaccurate, but more sophisticated models have not been developed [13]

At higher pressures, the gas molecules begin to interact and exert a viscous drag force on the beam Newell [24] also developed a first-order model based on gas pumping from between a cantilever and a substrate when the gap separation, g, is less than the cantilever width, b For the case of viscous damping, Q is given by

$$Q_u = \frac{2\pi f}{1\,03} \rho b \frac{h}{\mu} \left(\frac{g}{b}\right)^3 \quad (2)$$

where μ is the viscosity of the gas Due to the cover, pumping must occur between both top and bottom gaps Therefore, eqn (2) should be divided by at least a factor of two Assuming $\mu = 1\,8 \times 10^{-5}$ N s/m^2 (air) and the nominal beam values for the other parameters, the calculated Q is roughly 0 27 Although the calculation of Q by eqn (2) is no longer strictly valid for $Q \leqslant 5$, the implication is that the beam will not resonate under conditions of viscous air damping (at one atmosphere), as is observed experimentally

Another important resonator characteristic is the temperature dependence of the resonance frequencies Figure 6 shows the result of temperature cycling from room temperature to -60 °C, then up to $+160$ °C The resonator chip was supported only by its 0 001" gold lead wires to minimize stresses induced by the package The apparent

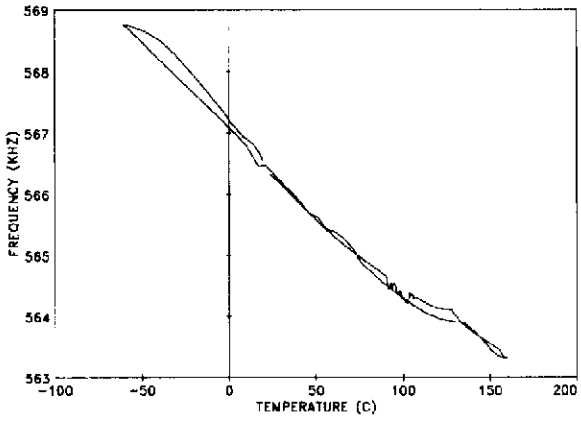

Fig 6 Oscillator frequency as a function of temperature for a 'floating die' device that was suspended by 1 mil gold wires and cycled between -60 and $+160$ °C

temperature hysteresis during and after temperature cycling is an experimental artifact caused by temperature differences between the temperature sensor and the device under test The frequency shift with temperature corresponds to a temperature coefficient of -50 ppm/°C for the linear region between -10 and $+100$ °C

The temperature dependence of the frequency is almost entirely due to the temperature dependence of Young's modulus, E, and is given by [16, 19]

$$\frac{1}{f_r}\frac{df_r}{dt} = \frac{1}{2E}\frac{dE}{dT} + \frac{1}{2}\alpha \quad (3)$$

where α is the linear coefficient of expansion This result follows directly from the simplest model of the beam behavior, based on the Rayleigh–Ritz method discussed below The temperature dependence of Young's modulus for polysilicon can be deduced from data on the elastic constants of silicon [20], and gives a value of -38 ppm/°C for the first term in eqn (3) Thus, eqn (3) predicts a temperature coefficient of -36 ppm/°C which is in reasonable agreement with experiment Single-crystal silicon beam resonators have been reported to have frequency coefficients of about -45 ppm/°C [3] and -29 ppm/°C [16] Torsional modes have a larger coefficient [18] We noted some variations between samples, which could be attributed to very small temperature-dependent external stresses caused by the sample supports, since the resonators are extremely sensitive to stress We conclude that the temperature effects are in reasonable agreement with theory and with those in single-crystal silicon,

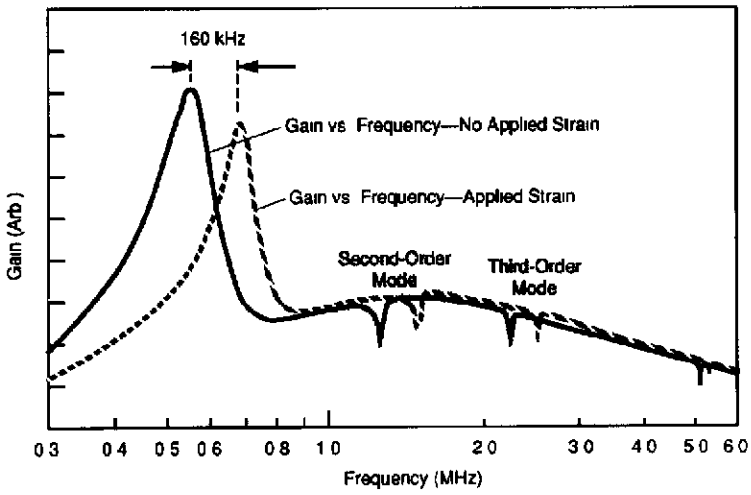

Fig 7 Higher-order modes All the devices tested showed a number of modes, which can be difficult to find by sweeping the frequency, except in low-Q devices such as this one

and that great care must be taken in order to find any differences that may exist

Characteristic frequencies

One of the most interesting aspects of the microbeam resonators is the observation of higher-order modes In high-Q devices these can be difficult to find with a digitally controlled frequency-synthesized drive voltage Figure 7 shows the first three bending modes of a low-Q microbeam A chip was mounted as a cantilever so that a bending force could be applied by deflecting the tip of the cantilever with a micrometer Figure 8 shows the frequency shifts due to the applied strain Table 1 gives frequencies of a strained and unstrained high-Q device, and compares the values with a fit to the theoretical model

Previous analyses of resonant microbeams have relied on approximate methods (e g , Rayleigh Ritz) to solve for the frequency of a doubly clamped beam with axial loads [7, 8] Energy methods such as Rayleigh–Ritz will yield an upper bound to the actual eigenvalue Results can be very good for the fundamental frequency, with a displacement function that is symmetric and satisfies the kinematic boundary conditions Accurate values for the second harmonic have also been obtained by assuming that the second mode is antisymmetric with a node exactly at midspan For any higher modes, the locations of the node points

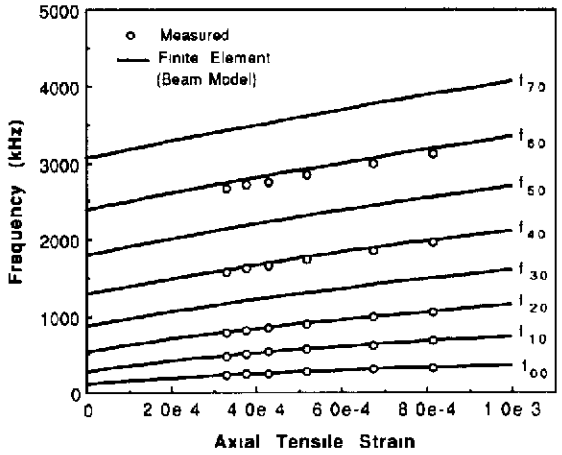

Fig 8 Frequency as a function of strain The theoretical curves show the frequencies of the planar bending modes as a function of total axial strain for the beam of Table 1 The experimental frequencies were measured on a cantilever sample with the external strain applied by a micrometer

are not necessarily known, and thus the errors in frequency estimates from Rayleigh–Ritz can be expected to increase accordingly Correlation of experimental data with analytical and numerical results depends not only on the fundamental frequency but on higher modes as well The theoretical solution for the one-dimensional response of the beam has been determined in closed form In addition, to substantiate these results, finite-element models of both a beam and a plate have been used to refine the frequency values and address the three-dimensional nature of the problem

TABLE 1 Frequencies (kHz) for a 400 μm × 40 μm × 1 8 μm beam in tension

Nodal pattern	Experimental data	Euler beam theory	Finite-element beam model	Finite-element plate model
(0,0)	303 9	303 7	303 6	303 8
(1,0)	626 7	628 8	628 7	629 1
(0,1)				648 5
(2,0)	985 7	993 6	993 3	994 5
(1,1)				1305 9
(3,0)		1412 0	1411 5	1414 3
(4,0)	1863 0	1893 9	1892 9	1898 6
(2,1)				1981 3
$(0,0)_v$[a]				2037 8
(5,0)		2445 7	2443 3	2454 4
(3,1)				2683 1
(6,0)	3000 2	3071 9	3068 4	3086 7
(4,1)				3418 0
(7,0)		3775 5	3772 4	3799 5
(5,1)				4194 9

[a]Beam bending about the major cross-section axis

For the analytical beam model, the transcendental frequency equation for a clamped–clamped beam with a constant axial tension can be found in the literature [26, 27] This closed-form solution is based upon classic Bernoulli Euler theory, which does not include shear and rotary inertia effects Defining the dimensionless tensile force as $U = Tl^2/12EI$ and the dimensionless flexural frequency as $\Omega = \omega l^2\alpha$, the characteristic equation can be expressed as

$$\Omega + U \sinh(U + \sqrt{U^2 + \Omega^2})^{1/2} \times \sin(-U + \sqrt{U^2 + \Omega^2})^{1/2} - \Omega \cosh(U + \sqrt{U^2 + \Omega^2})^{1/2} \times \cos(-U + \sqrt{U^2 + \Omega^2})^{1/2} = 0 \quad (4)$$

Here T, l, E, I and ω represent the tensile force, length, elastic modulus, cross-section moment of inertia and flexural rigidity, respectively The parameter α is given by $\alpha = (EI)^{1/2}/\rho A$, in which ρ is the material density and A is the cross-sectional area

Specific results are presented in Table 1 for a beam 400 μm long, 40 μm wide and 1 8 μm thick with an elastic modulus of 1 61 dyne/cm^2, Poisson's ratio of 0 26 and density equal to 2 33 g/cm^3 Frequencies are associated with a pair of numbers identifying the nodal pattern The first is the number of node lines in the transverse direction (excluding the ends), the second is the number of node lines in the axial direction Euler beam-theory models the planar flexural response about the minor axis and thus such patterns are designated as $(n, 0)$ Experimental and theoretical results are matched for the fundamental frequency by using a tensile load of 782 6 dyne corresponding to an axial strain of $6\,75 \times 10^{-4}$, which includes $3\,23 \times 10^{-4}$ of internal strain This is subsequently used to determine the theoretical values for the higher frequencies

It should be noted that for very high frequencies (characterized by short wavelengths), shear deformation and rotary inertia become increasingly important Both contribute to a reduction in frequencies, compared with classical theory Consequently, a finite-element analysis which included these additional effects was performed for the planar beam response Results are also presented in Table 1 Small corrections can be seen for frequencies f_{60} and f_{70}, however, these deviations would increase for higher modes The finite-element beam model was also used to show the effect of axial strain on the resonance frequencies (Fig 8) Additional experimental data are shown on the Figure for the symmetric (planar) modes as well as for the first antisymmetric mode Higher antisymmetric modes are not observed with the nearly uniform excitation source (Nonuniformities in the source could excite not only planar antisymmetric modes but also three-dimensional oscillations) The fact that the computational results are higher than the experimental may be attributable to the slightly stiffer finite-element model, i e , the model represents the supports as rigid

In order to develop a more complete understanding of the response of the resonator, the analysis was extended to three dimensions by using a finite-element plate model With this model the entire spectrum of frequencies was determined, i e , frequencies corresponding to all possible nodal patterns Table 1 shows a comprehensive listing of these patterns with the associated frequencies for the first 15 modes The results are in direct correlation with the experimental data, the theoretical beam model and the finite-element beam model The actual ordering of the nodal patterns is dependent upon the plate dimensions and the applied axial strain Figure 9 illustrates some of the higher-order modes listed in Table 1 It is worth noting that the in-plane mode $(0, 0)_v$ is

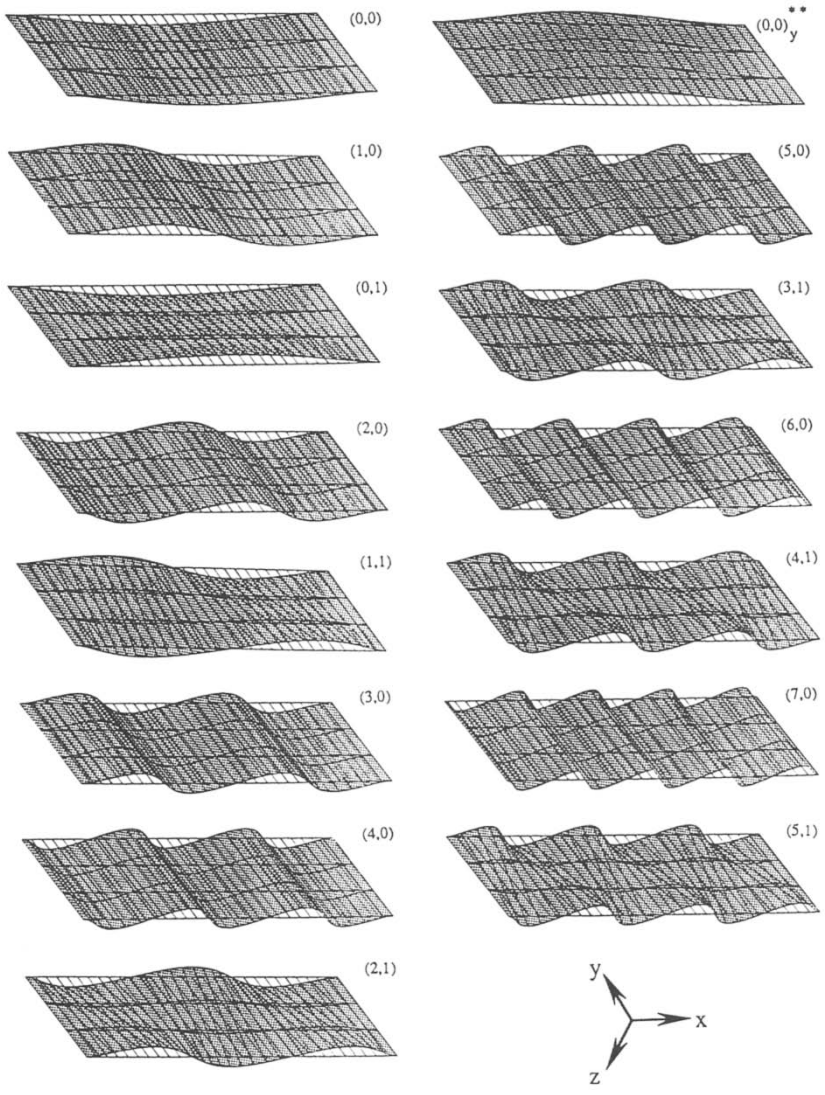

Fig 9 Selected mode shapes The labeling corresponds to Table 1 Generally, element displacements are along the z direction except for the (0, 0), mode, where displacement is along the y direction

not included in the usual analysis of plates [28] However, it can be calculated by one-dimensional beam theory Future tests will be aimed at exciting and measuring these plate-like modes to further identify the characteristics of the resonator

Conclusions

The excellent agreement between the experimental data and the theoretical models for the higher-order modes shows that the device is indeed well behaved In Fig 8, for example, the five observed frequencies are fitted to the theory using only one adjustable parameter, the applied strain Using the fit, this strain can be determined much more accurately than it can be measured The residual internal strain of the microbeam can also be determined with high accuracy from a measurement of one or more higher-mode frequencies Thus, the resonant microbeam is, in effect, a self-calibrated strain gage, with the gage factor, $\Delta f/f\varepsilon$, given by the theoretical fit, where Δf is the frequency shift of the fundamental mode and ε is the applied strain $\Delta l/l$ In Fig 8, for example, the gage factor is 1100 This compares to gage factors ($\Delta R/R/\varepsilon$) for

piezoresistors that are typically less than five for metals and less than 125 for single-crystal silicon In actual sensor applications, it is not the strain that must be calibrated, but rather the sensed variable, e g , pressure or acceleration Nevertheless, measurement of higher-order modes may be useful in characterizing device performance and in monitoring variations in the mechanical properties

Acknowledgements

We wish to acknowledge the leadership of Ben Hocker and Norm Foss in establishing the Honeywell–University of Wisconsin collaboration Bob Pearson and Bob Matthys developed the oscillator circuits and Cindy Bassett and Steve Johnston were responsible for the test data presented

References

1 R Frische, Vibratory pressure sensors, *Scientific Honeyweller*, (Fall) (1987) 79–84
2 M A Schmidt and R T Howe, Silicon resonant microsensors, *Ceram Eng Sci Proc , 8* (1987) 1014–1034
3 R A Buser and N F de Rooij, Resonant silicon structures, *Sensors and Actuators, 17* (1989) 145–154
4 K Ikeda, H Kuwayama, T Kobayashi, T Watanabe, T Nishikawa, T Yoshida and K Harada Silicon pressure sensor integrates resonant strain gauge on diaphragm, *Sensors and Actuators, A21–A23* (1990) 146–150
5 M W Putty S-C Chang, R T Howe, A L Robinson and K D Wise, Process integration for active polysilicon resonant microstructures, *Sensors and Actuators, 20* (1989) 143–151
6 H Guckel J J Sniegowski and T R Christensen, Construction and performance characteristics of polysilicon resonating beam force transducers, *Proc 3rd Toyota Conf on Integrated Micro Motion Systems, Nissin, Aichi, Japan*, 1989, pp (23-1)–(23-10)
7 J J Sniegowski H Guckel and T R Christensen, Performance characteristics of second generation polysilicon resonating beam force transducers, *IEEE Solid State Sensor and Actuator Workshop, Hilton Head Island SC, USA, June 1990*, pp 9–12
8 H Guckel, J J Sniegowski, T R Christenson and F Rossi, The application of fine-grained, tensile polysilicon to mechanically resonant transducers *Sensors and Actuators, A21–A23* (1989) 346–356
9 H Guckel, Surface micromachined pressure transducers, *Sensors and Actuators A, 28* (1991) 133–146
10 J J Sniegowski, Design and fabrication of the polysilicon resonating beam force transducer, *Ph D Thesis*, Dept of Nuclear Engineering and Engineering Physics, University of Wisconsin, Madison, WI, 1991
11 J D Zook, D W Burns, H Guckel, J J Sniegowski, R I Englestad and Z Feng, Resonant microbeam strain transducers, *Tech Digest, 6th Int Conf Solid-State Sensors and Actuators (Transducers '91), San Francisco, CA, USA, June 24–28, 1991*, pp 529–533
12 K Petersen, F Pourahmadi, J Brown, P Parsons, M Skinner and J Tudor, Resonant beam pressure sensor fabricated with silicon fusion bonding, *Tech Digest, 6th Int Conf Solid-State Sensors and Actuators (Transducers '91) San Francisco, CA, USA, June 24–28 1991*, pp 664–667
13 B Hok and K Gustafsson, Vibration analysis of micromechanical elements, *Sensors and Actuators, 8* (1985) 235–243
14 D DeRoo, Determination of Young's modulus of polysilicon using resonant micromechanical beams, *M S Report*, Dept of Electrical and Computer Engineering, University of Wisconsin, Madison, WI, January 1988
15 T V Roszhart, The effect of thermoelastic internal friction on the *Q* of micromachined silicon resonators, *IEEE Solid State Sensor and Actuator Workshop, Hilton Head Island, SC, USA, June 1990*, pp 13–16
16 M J Tudor, M V Andres, K W H Foulds and J M Naden, Silicon resonator sensors interrogation techniques and characteristics, *IEEE Proc , 135D* (1988) 364–367
17 G Stemme, Resonant silicon sensors, *J Micromech Microeng , 1* (1991) 113–125
18 R A Buser and N F de Rooij, Very high *Q*-factor resonators in monocrystalline silicon, *Sensors and Actuators, A21–A23* (1990) 323–327
19 H A C Tilmans, S Bouwstra, D J IJntema and M Elwenspoek, A differential resonator design using a bossed structure for applications in mechanical sensors, *Sensors and Actuators A, 26* (1991) 385–393
20 D W Burns, Micromechanics of integrated sensors and the planar processed pressure transducer, *Ph D Thesis*, Dept of Material Science, University of Wisconsin, Madison, WI, 1988
21 H J Pain, *The Physics of Vibrations and Waves*, Wiley, Chichester, 3rd edn , 1983, p 362
22 E P Eernisse, R W Ward and R B Wiggins, Survey of quartz bulk resonator sensor technologies, *IEEE Trans Ultrasonics, Ferroelectrs Freq Control, UFFC-35* (1988) 323–330
23 L D Clayton, E P Eernisse, R W Ward and R B Wiggins, Miniature crystalline quartz electromechanical structures, *Sensors and Actuators, 20* (1989) 171–177
24 W E Newell, Miniaturization of tuning forks, *Science, 161* (1968) 1320–1326
25 R G Christian, The theory of oscillating-vane vacuum gauges, *Vacuum, 16* (1966) 175
26 D J Gorman, *Free Vibration Analysis of Beams and Shafts*, Wiley, New York, 1975
27 A Bokaian, Natural frequencies of beams under compressive axial loads, *J Sound Vibr , 266* (1988) 49–65
28 D J Gorman, *Free Vibration Analysis of Rectangular Plates*, Elsevier, New York, 1982